ISSN: 1813-4890

Residual Network-Based Dual-Branch Time-Frequency Domain Multipath Detection and Suppression

Lingli Tong, Junpeng Rao

School of Artificial Intelligence, Hubei University, Wuhan 430415, China

Abstract

To address multipath interference in Global Navigation Satellite System (GNSS) signals, this paper proposes a deep learning-based multipath detection and suppression method utilizing a dual-branch feature extraction fusion mechanism. First, GNSS signal samples with and without multipath interference are generated through modeling, and their time-domain and frequency-domain features are extracted. Subsequently, the time-domain and frequency-domain data undergo separate feature extraction through a dual-branch architecture. The time-domain branch utilizes a Residual Network (ResNet) integrated with Efficient Channel Attention (ECA), while the frequency-domain branch employs a Bidirectional Long Short-Term Memory (BiLSTM) network. Subsequently, a dynamic attention fusion module (AttentionFusion) dynamically weight-assigns the two feature branches to achieve optimized integration of time-frequency domain features. Experimental results demonstrate that this method exhibits strong learning and generalization capabilities in both multipath detection and suppression, overcoming the limitations of approaches relying solely on time-domain analysis.

Keywords

GNSS; multipath; residual network; dynamic attention fusion module; dual-branch.

1. Introduction

Multipath interference is a common issue in global satellite navigation systems. It occurs when radio signals are reflected, refracted, or scattered by objects in the surrounding environment during transmission, causing multiple signal paths to arrive simultaneously at the receiving device. When multipath signals overlap with the direct signal, interference manifests as signal amplitude amplification or attenuation, phase distortion, and other anomalies. Such interference not only affects signal correlation characteristics but may also cause pseudorange measurement errors, thereby reducing the positioning accuracy of navigation systems. In complex environments such as urban areas, high-rise dense zones, or mountainous regions, the multipath effect is particularly pronounced, becoming a significant error source that cannot be ignored in GNSS systems. Therefore, effective detection and suppression of multipath interference have become key research topics for enhancing the accuracy and robustness of navigation and positioning technology systems [1].

Among traditional signal processing methods, time-domain processing predominantly employs correlator-based output correlation function techniques.[2] proposes a novel code tracking loop multipath suppression scheme. [3] introduces a method utilizing BOC signals to effectively suppress GNSS multipath effects. [4] introduced a fast offset correlator technique, combining fast and offset correlators in a complementary manner to mitigate BOC signal multipath. [5] proposed a dual high-resolution correlator technique for BOC signal code element and subcarrier multipath errors. In frequency-domain processing, [6] employed two FFT-based detectors as GPS multipath detection techniques, [7] performs wavelet transformation on signals generated by correlators, followed by neural network learning on the transformed

ISSN: 1813-4890

signals. Among statistical inference methods, [8] proposes a maximum likelihood estimation-based power-distortion detection method that analyzes distortion levels in correlation functions to detect and classify multipath, spoofing, and interference in GNSS signals.

2. Signal Generation Model

The user's position is calculated by a global navigation satellite system receiver using trilateration technology, primarily by measuring the geometric distance from the receiver antenna to known satellites. Compared to direct signals, multipath signals introduce additional delays; therefore, the resulting composite signal is essentially the superposition of direct and multipath signals.

In the time domain, the direct signal is represented as：

$$S_{time}^{LOS}(\tau,t) = A\sin c(\frac{\tau-\tau_0}{T_c})\cos(2\pi f_0 t+\theta_0)+n(t) \tag{1}$$

where A is the main beam signal amplitude, τ_0 is the main beam delay, f_0 is the main beam frequency, θ_0 is the main beam phase, $sinc$ is the main lobe of the correlator output, t is the time sampling point, and T_c is the codeword length. $n(t)$ represents Additive White Gaussian Noise (AWGN), reflecting receiver-related thermal noise, commonly referred to as antenna port noise[9].

Due to the distortion of the direct signal caused by multipath effects, the above formula alone is insufficient for effectively modeling the received signal. Multipath signals are modeled in the same manner as the direct signal. However, multipath signals introduce additional delays during generation, thus:

$$\mathrm{S_{time}^{NLOS}}(\tau,\mathrm{t}) = \alpha\sin \mathrm{c}(\frac{\tau-\tau_{\mathrm{m}}}{\mathrm{T_c}})\cos(2\pi \mathrm{f_m t}+\theta_{\mathrm{m}})+\mathrm{n(t)} \tag{2}$$

Among these, α represents the multipath amplitude relative to the main path, typically ranging from 1 to 2; τ_m denotes multipath delay; f_m indicates multipath frequency offset; and θ_m signifies multipath phase.

Therefore, the received signal is the superposition of the direct signal and the multipath signals:

$$\mathrm{S(t)} = \mathrm{S_{time}^{LOS}}(\tau,\mathrm{t})+\sum_{\mathrm{i=0}}^{\infty}\mathrm{S_{time}^{NLOS}}(\tau,\mathrm{t_i})+\mathrm{n(t)} \tag{3}$$

At this point, the received signal is multiplied by the local subcarrier, splitting the signal into two channels:

$$\begin{aligned} I_{NLOS} &= A\cos(\pi(\Delta f-\Delta\widetilde{f})T_i+(\theta_r-\widetilde{\theta}_r))\times\sin c(\pi(\Delta f-\Delta\widetilde{f})T_i)+n_I(t) \\ Q_{NLOS} &= -A\sin(\pi(\Delta f-\Delta\widetilde{f})T_i+(\theta_r-\widetilde{\theta}_r))\times\sin c(\pi(\Delta f-\Delta\widetilde{f})T_i)+n_Q(t) \end{aligned} \tag{4}$$

Among these, $\mathrm{A}=\frac{\mathrm{DT_i}}{2}\sqrt{\frac{\mathrm{C}}{2}}\mathrm{K}(\widetilde{\tau}-\tau)$， $\widetilde{\tau}-\tau$ represents propagation delay estimation error, $K(*)$ denotes the autocorrelation coefficient of the PRN code, $\Delta f-\Delta\widetilde{f}$ signifies Doppler shift error, $\theta_r-\widetilde{\theta}_r$ indicates phase estimation error, and $n_I(t)\sim N(0,\frac{N_0T_i}{16})$ and $n_Q(t)\sim N(0,\frac{N_0T_i}{16})$ are two independent identically distributed white noise components.

After the correlator generates the time-domain image, a two-dimensional Fourier transform (2D FFT) is performed to obtain its frequency-domain feature map.

ISSN: 1813-4890

In the time domain, when the received signal contains only the direct path component, the correlator output typically manifests as a well-defined, concentrated primary correlation peak. Its peak corresponds to the signal's minimum propagation delay time and serves as a crucial reference for code synchronization and pseudorange estimation in the receiver. When multipath interference is present, one or more additional correlation peaks appear in the output alongside the primary peak, exhibiting varying degrees of time delay offset relative to the primary peak. The superposition of multipath components not only alters the overall shape of the correlation function but may also cause peak broadening, distortion, or peak displacement, thereby adversely affecting delay estimation accuracy.

In the frequency domain, the spectral structure corresponding to the direct signal is typically well-defined, with energy concentrated within a finite frequency range and a relatively smooth and stable spectral shape. When multipath signals are present, phase differences and time delays introduced by different propagation paths generate significant interference effects in the frequency domain. This redistributes the originally concentrated spectral energy, manifesting as spectral broadening, increased energy fluctuations, and the enhancement or attenuation of specific frequency components. Under conditions of strong multipath or significant path variations, multiple broad peaks with concentrated energy or spectral overlap may appear, significantly altering the signal's frequency domain structural characteristics.

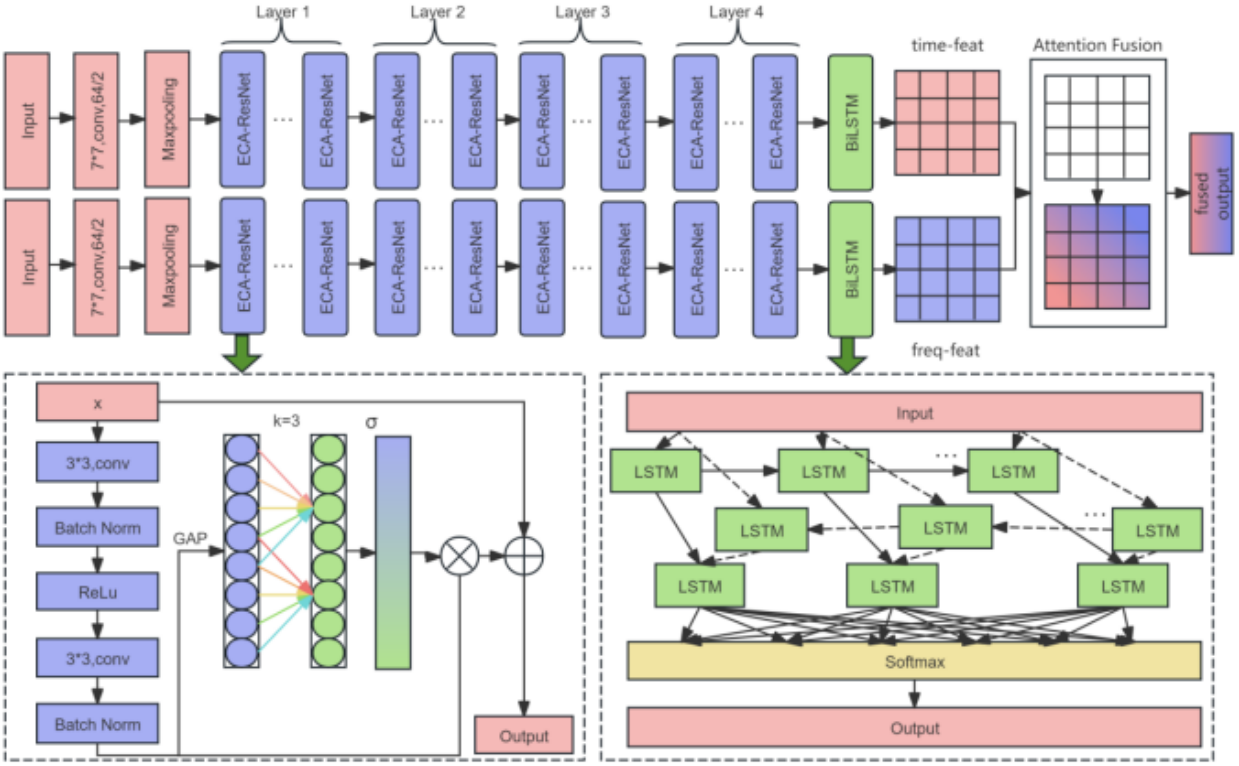

Fig.1 Overall Architecture of the Dual-Branch Network

3. Network Model

To fully leverage the complementary characteristics of multipath signals in both the time and frequency domains within GNSS signals, this paper proposes a dual-branch ECA-ResNet-BiLSTM fusion network architecture.This model primarily consists of two feature extraction branches, an attention fusion module, and a regression/classification prediction module. The residual module configuration across network layers is [2, 2, 2, 2]. The input consists of a 4-channel image, corresponding to the I/Q channels in the time domain and the I/Q channels in the frequency domain. The time-domain branch network extracts dynamic features of the original signal in the time dimension, while the frequency-domain branch network extracts

ISSN: 1813-4890

spectral distribution features. The fusion module employs an adaptive attention mechanism to perform weighted fusion of time-domain and frequency-domain features, thereby enhancing the network's robustness against multipath interference and nonlinear distortion.

3.1. Dual-Branch ECANet Fusion Network

This network is based on the ResNet architecture, incorporating an ECA module and a BiLSTM module to construct each branch. These branches are designed to extract features from temporal-domain images and frequency-domain images, respectively.

Multipath signals typically exhibit complex trailing or distortion in the correlator output image, with relatively weak features that are easily overlooked by shallow networks. The ResNet architecture introduces a deep network structure, increasing the number of layers while preserving information. This enables the model to learn more complex spatial features, thereby identifying subtle multipath characteristics[10].

The time-domain image reveals the position, shape, and secondary peak locations of the main correlation peak. Therefore, the deep convolutional structure of the ResNet network can accurately extract the main peak region and detect weak multipath trailing phenomena across the entire image. In the frequency-domain image, multipath signals exhibit spectral asymmetry. ResNet can extract local frequency-domain models through multiple convolutional layers and then integrate global frequency features via residual connections. When analyzing multipath signals solely in the time domain, propagation delays from different paths may be extremely close. Due to the limited resolution of time-domain signals, overlapping signals with small delay differences become difficult to distinguish and detect effectively. Moreover, multipath signals exhibit not only varying delays but also frequency shifts and phase differences. Purely temporal analysis struggles to capture these concurrent frequency and phase variations. Consequently, temporal analysis faces limitations in multipath signal detection, particularly in environments with small multipath delay differences, strong noise, and complex phase/frequency variations. Thus, a dual-branch architecture is employed for comprehensive temporal and frequency domain analysis of multipath signals.

The ECA module employs a lightweight attention mechanism to weight the importance of different channels, directing the network to focus on channels with prominent multipath features while suppressing irrelevant noise channels. Instead of using fully connected layers, it models interactions between local channels via one-dimensional convolutions, enabling more effective extraction of fine-grained channel features related to multipath. Crucially, this network employs a dual-branch architecture where both branches share identical structures but process signals with distinct distributions. The ECA module captures primary and secondary peak features in the time-domain branch while emphasizing spectral broadening and distortion features in the frequency-domain branch. Consequently, the ECA module dynamically adjusts its attention strategy based on input image variations. Compared to traditional attention mechanisms, the ECA module does not increase parameter dimensions, reduces computational complexity, and improves learning efficiency.

Furthermore, multipath signals manifest as time-domain delays or frequency-domain expansions in correlator images—features exhibiting continuity along a single direction. To capture temporal and contextual information within these features, a BiLSTM module is integrated after ECA-ResNet feature extraction. This BiLSTM module perceives change patterns across multiple preceding and subsequent feature points, thereby capturing temporal or spatial relationships between features.

3.2. Attention Feature Fusion

Regarding fusion methods, existing approaches primarily employ strategies such as static weight fusion or feature concatenation fusion. In static weight fusion, weight values are fixed

ISSN: 1813-4890

before training and cannot be dynamically adjusted based on input data features, making it impossible to distinguish the importance of different feature channels. If a feature branch is contaminated by noise, static weights cannot automatically suppress its negative impact. Consequently, the complementary nature of temporal and frequency domain features remains underutilized, and the model struggles to learn cross-domain correlated features. Feature concatenation fusion, however, merely involves the simple superposition of features from two branches. This increases the dimensionality of the resulting features, leading to an increase in parameters for subsequent processing and excessive computational load. Moreover, simple concatenation fails to fully leverage the correlations between different features. Furthermore, different branches may contain overlapping information, and direct concatenation can result in redundant information[11].

This network employs a dynamic feature fusion module based on an attention mechanism. Within this module, the feature vectors derived from both the time-domain and frequency-domain images are concatenated to form a new feature matrix.

$$\mathrm{X}_{\mathrm{fused}} = \mathrm{concat}(\mathrm{X}_{\mathrm{time}}, \mathrm{X}_{\mathrm{freq}}) \tag{5}$$

Input the concatenated feature vectors into a 1×1 convolutional layer to compress the concatenated feature maps from two channels to one channel. Then, fuse the merged images using a nonlinear function. Subsequently, adjust the output with another 1×1 convolutional layer to produce a weight map suitable for weighted fusion.

$$\hat{X} = Conv_2(\mathrm{Re}\,lu(Conv_1(X_{fused}))) \tag{6}$$

Specifically, $Conv_1$ is used for the number of compressed channels, while $Conv_2$ adjusts the output to prepare for generating the weight map. The activation function performs a nonlinear transformation to ensure negative values are eliminated.

Finally, the output weight map is compressed to the range [0, 1] via the sigmoid activation function. This enables weighted fusion to be applied to the final output, representing the weighting coefficients:

$$\alpha = Sigmoid(\hat{X}) \tag{7}$$

The resulting weight values represent the proportion of temporal or frequency domain information to be retained during the fusion process.

Finally, the temporal and frequency domain information undergoes dynamic weighted summation based on the attention weights.

$$fused = \alpha \cdot X_{time} + (1-\alpha) \cdot X_{freq} \tag{8}$$

During the multipath suppression stage, the fused weight values are applied to the target image, ensuring that the fusion weights for both the time-domain and frequency-domain images of the target image align with those of the predicted image. This alignment facilitates image similarity comparisons during the multipath suppression stage.

4. Analysis of Simulation Results

4.1. Experimental Data Processing

In this study, to validate the effectiveness of the proposed model in GNSS multipath detection and suppression tasks, it is necessary to construct a sufficiently large and controllable dataset. However, directly acquiring large-scale real GNSS receiver data presents significant challenges in practical implementation. On one hand, data collection in real-world environments imposes stringent requirements on receiving equipment, experimental sites, and testing conditions. On the other hand, the collection process is time-consuming, costly, and difficult to rigorously replicate, making it challenging to meet the demands of deep learning models for sample

ISSN: 1813-4890

quantity and diversity. Therefore, this paper utilizes a publicly available artificial signal generator [12]. The generator produces datasets comprising four sample categories: time-domain direct signal images, time-domain multipath signal images, frequency-domain direct signal images, and frequency-domain multipath signal images. Each sample category includes both I-channel and Q-channel images. Experimental data is generated by the signal generator in matrix form. All datasets share the following variables: the PRN code used is the C/A code with a code rate of 1.023 MHz, a code length of 1023, and a code period of 1 ms. Due to the discrete nature of digital signal processing, the signal is sampled at a frequency of 20 MHz. The range for multipath delay was set to $(-1.5T_c, 5T_c)$, the Doppler shift range to $\delta f < \left|\min(5.5/T_i, 800 + 2.5/T_i)\right|$, the coherent integration time to 20 ms, the phase shift range to $(0, 2\pi)$, and the signal-to-noise ratio to 40 dBHz. These parameters yielded favorable results in the experiments.

The dataset constructed for this study comprises 50,000 sets of time-frequency domain samples. Each sample consists of a pair of I and Q images in the time and frequency domains, respectively, with a fixed image size of 80×80 pixels. Prior to training, the dataset was partitioned into training, test, and validation sets at a ratio of 6:2:2.

During the multipath detection phase, the time-domain branch takes the time-domain multipath signal image as input and the corresponding multipath delay parameter as the supervised label, outputting the predicted delay estimate. The frequency-domain branch takes the frequency-domain multipath signal image as input, also using multipath delay as the label, to obtain the corresponding prediction result. Finally, the predicted delays from both branches are fused (by averaging) to obtain the dual-branch model's output. This is then compared with the true delay labels to validate the model's effectiveness in multipath delay estimation. Using the same training and evaluation approach, the model's overall performance in multipath parameter detection is verified by employing Doppler frequency shift and carrier phase shift as supervised labels, respectively.

During the multipath suppression phase, the model first processes the detected multipath parameters before prediction. The three scalar parameters—delay, frequency offset, and phase shift—are each subjected to two-dimensional expansion, generating 80×80 parameter feature maps that are introduced into the model as auxiliary prior information. The model's input comprises five images: the time-domain multipath signal image, the frequency-domain multipath signal image, and the two-dimensional expanded images corresponding to delay, frequency offset, and phase shift. Specifically, the time-domain branch receives a four-channel input comprising the time-domain multipath image and the three parameter feature maps. It is trained using the time-domain uncorrupted signal image as the supervised label, ultimately outputting the corresponding time-domain uncorrupted prediction image. The frequency-domain branch employs the same architecture and training strategy, taking the frequency-domain multipath image and parameter feature maps as input, with the frequency-domain uncorrupted signal image as the label, to generate the frequency-domain uncorrupted prediction result. Finally, the prediction results from the time-domain and frequency-domain branches are integrated through a weighted fusion mechanism to obtain the final multipath suppression output. This output is then compared with the true multipath-free image using similarity analysis to validate the effectiveness and robustness of the proposed method in multipath suppression tasks.

4.2. Multipath Detection Phase

To evaluate the model's fit with observational data, this paper employs the coefficient of determination as the assessment metric, with a value range of . In extreme cases, when , it indicates the prediction model completely fails to match the observational data; when , it

ISSN: 1813-4890

indicates the prediction model perfectly fits the observational data, demonstrating excellent explanatory power. The following figure shows the results trained with time delay, frequency offset, and phase shift as labels, respectively:

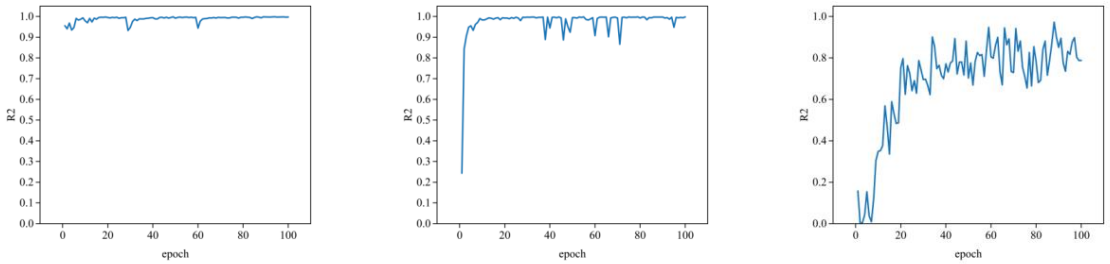

Fig.2 Training results labeled as time delay (left), frequency offset (middle), and phase offset (right)

As shown in Table 1, models were trained using delay, frequency offset, and phase offset as labels for comparison. Most existing multipath parameter estimation models are trained using time-domain image data. In this experiment, traditional CNN architectures (CNN, CNN-LSTM, EfficientNet, ResNet) all achieved certain recognition performance on this dataset. Among them, ResNet demonstrated good performance under time-domain images. Further introduction of modules such as the ECA attention mechanism and LSTM structure improved model performance to varying degrees. However, the proposed method differs from previous approaches that relied solely on temporal information. Instead, it adopts a joint modeling approach combining both temporal and frequency-domain images. Experimental results demonstrate that the proposed dual-branch fusion model achieves significantly higher estimation accuracy for all three key parameters compared to existing methods, validating the effectiveness and feasibility of dual-domain fusion for GNSS multipath detection.

Table1 Comparison of Detection Accuracy Across Different Models

Method	$\triangle\tau$	$\triangle f$	$\triangle\theta$
VGG16	60.63	57.72	20.38
CNN	91.09	87.16	36.14
CNN-LSTM	98.54	97.35	58.62
EfficientNet	95.37	92.16	65.74
ResNet	97.44	97.21	56.32
Ours	99.84	99.80	86.15

To further validate the effectiveness of each individual module within this model, ablation experiments were designed to compare the performance of different components. As shown in Table 2, the training process employed delay, frequency offset, and phase offset as regression labels respectively:

Table2 Comparison Results of Multipath Detection Ablation Experiments

Index	Dual Branch	Time-Branch	Frequency-Branch	ECA-ResNet-BiLSTM	Accuracy/%		
					$\triangle\tau$	$\triangle f$	$\triangle\theta$
1	√			√	99.84	99.80	86.15
2		√		√	99.81	99.61	83.15
3			√	√	93.65	85.15	56.37

After training the model on a single time-domain branch, compared to the dual-branch structure in the time-frequency domain, the time-domain branch model showed a smaller accuracy gap in time delay and frequency offset prediction, though accuracy still decreased by 0.03% and 0.19% respectively. Accuracy in phase offset prediction decreased by 3%. When training the model in a single frequency-domain branch, compared to the dual-branch structure

ISSN: 1813-4890

in both time and frequency domains, the accuracy of the frequency-domain branch decreased by 6.19%, 14.65%, and 29.78% for time delay, frequency offset, and phase offset prediction, respectively. Since phase offset reflects carrier signal phase variations-complex and subtle high-frequency features-accurate modeling typically requires joint support from both time-domain and frequency-domain information. Performance in phase-offset prediction tasks significantly deteriorated when using either the time-domain or frequency-domain branch alone, indicating that single-type features cannot fully capture critical phase-change information. Integrating time-frequency domain features is therefore crucial for phase-offset modeling.

4.3. Multipath Suppression Analysis

To evaluate the effectiveness of the proposed multipath suppression method in preserving signal structural information, this paper introduces the Structural Similarity Index (SSIM) as a metric. SSIM primarily measures structural consistency between images, better reflecting image quality and perceptual similarity than traditional Mean Squared Error (MSE). The following figure shows the SSIM values and loss values for the two multipath suppression results:

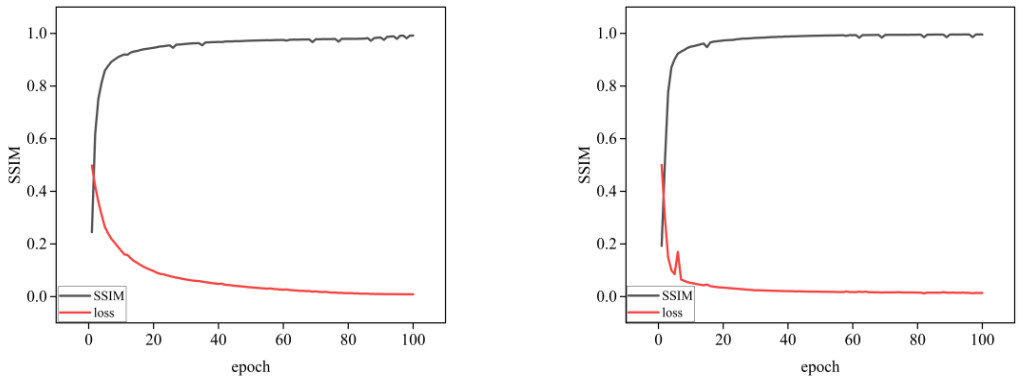

Fig.3 I-path (left), Q-path (right) SSIM values and loss values

Table 3 presents a comparison of results from existing methods. As shown in the table, under identical conditions, the results obtained in this study demonstrate good similarity in both the I and Q channels of the multipath image:

Table3 Comparison of Inhibition Accuracy Across Different Models

Method	I	Q
CNN	53.19	59.56
CNN+LSTM	78.29	93.86
EfficientNet	75.73	76.13
ResNet	84.84	91.64
Ours	99.1	99.65

Similarly, the same ablation experiments were conducted during the multipath suppression phase, with the results shown in Table 4.

Table4 Comparison Results of Multipath Suppression Ablation Experiments

Index	Dual Branch	Time-Branch	Frequency-Branch	ECA-ResNet-BiLSTM	Accuracy/%	
					I	Q
1	√			√	99.1	99.65
2		√		√	97.52	99.30
3			√	√	87.46	90.62

The comparison results from the ablation experiments show that the model incorporating a dual-branch structure achieved accuracy rates of 99.10% and 99.65% on the I-path and Q-path, respectively, significantly outperforming the single-branch structure. This demonstrates that integrating spatiotemporal domain information effectively enhances multipath suppression performance. When using only the time-domain branch, the accuracy rates for the I and Q channels were 97.52% and 99.30%, respectively. However, when using only the frequency-domain branch, the accuracy rates dropped significantly to 87.46% and 90.62%. This indicates that while frequency-domain features play a role in multipath interference identification, their effectiveness is limited when used alone. Compared to single-branch models, the dual-branch structure not only improves accuracy but also demonstrates better robustness in both I and Q channels, further validating the complementary nature of time-domain and frequency-domain features.

5. Conclusion and Summary

This paper proposes an ECA-ResNet-BiLSTM network model with dual branches in the time and frequency domains for detecting and suppressing multipath signals. The dual-branch architecture extracts time-domain and frequency-domain image features respectively. The ECA module applies adaptive weighting to channel importance, enabling the network to focus on prominent features related to multipath signals while suppressing irrelevant noise. Simultaneously, BiLSTM modules are incorporated into each branch to model feature sequences, capturing the continuity and temporal correlations of multipath signals and enhancing the recognition capability of weak signal components. During the feature fusion stage, a fusion module based on a dynamic attention mechanism is designed to weight and integrate time-domain and frequency-domain features. This allows the network to automatically adjust the fusion ratio according to the specific characteristics of the input signal, thereby improving the robustness of multipath detection and suppression. The dual-branch ECA-ResNet-BiLSTM model constructed in this paper fully leverages multi-modal information across time and frequency domains to achieve high-precision multipath detection and effective suppression. This provides reliable technical support for GNSS signal processing and positioning accuracy enhancement.

References

[1] Xue Z, Lu Z, Xiao Z, et al. Overview of multipath mitigation technology in global navigation satellite system[J]. Frontiers in Physics, 2022, 10: 1071539.

[2] Xu H, He C, Xu Y. A novel multipath mitigation scheme for GNSS BOC signals[C]//2011 7th International Conference on Wireless Communications, Networking and Mobile Computing. IEEE, 2011: 1-4.

[3] Alhussein F, Liu H. An Efficient Method for Multipath Mitigation Applicable to BOC Signals in GNSS[C]//2019 15th International Wireless Communications & Mobile Computing Conference (IWCMC). IEEE, 2019: 793-798.

[4] Tian Z, Cui X, Lu M. Multipath Mitigation for BOC Signals Based on Prompt-Assisted-Offset Correlator[J]. Remote Sensing, 2023, 15(4): 937.

[5] Tian Z, Cui X, Zhu Y, et al. Dual High-Resolution Correlators for Multipath Mitigation in BOC Signals[J]. IEEE Transactions on Aerospace and Electronic Systems, 2023, 59(5): 5012-5026.

[6] Amani E, Djouani K, Kurien A, et al. GPS multipath detection in the frequency domain[J]. arXiv preprint arXiv:1707.09770, 2017.

[7] Kim O J, Kee C. Wavelet and neural network-based multipath detection for precise positioning systems[J]. Mathematics, 2023, 11(6): 1400.

ISSN: 1813-4890

[8] Gross J N, Kilic C, Humphreys T E. Maximum-likelihood power-distortion monitoring for GNSS-signal authentication[J]. IEEE Transactions on Aerospace and Electronic Systems, 2018, 55(1): 469-475.

[9] Chen X, Shao Y, He D, et al. Reflection objects sensing and localization with GNSS multipath signals[C]//China Satellite Navigation Conference (CSNC 2021) Proceedings: Volume III. Springer Singapore, 2021: 203-214.

[10] Cho S, Seok H W, Kong S H. Mpcnet: Gnss multipath error compensation network via multi-task learning[C]//2023 IEEE Intelligent Vehicles Symposium (IV). IEEE, 2023: 1-6.

[11] Li Y, Daho M E H, Conze P H, et al. A review of deep learning-based information fusion techniques for multimodal medical image classification[J]. Computers in Biology and Medicine, 2024, 177: 108635.

[12] Blais A, Munin E, Couellan N. A synthetic GNSS correlator output generator. 2021, URL: https://github.com/AntoineBlaisENAC/Synthetic_GNSS_Correlator_ Output_Generator.git.